Giant dipole resonance studies in Ba isotopes at $E/A \approx 5$ MeV

C. Ghosh,[1] A. K. Rhine Kumar,[1,*] Balaram Dey,[1] V. Nanal,[1,†] R. G. Pillay,[1] P. Arumugam,[2] K. V. Anoop,[3] N. Dokania,[1] Abhijit Garai,[4] Ghnashyam Gupta,[1] E. T. Mirgule,[5] G. Mishra,[5] Debasish Mondal,[6,7] S. Pal,[3] M. S. Pose,[1] and P. C. Rout[5]

[1]*Department of Nuclear and Atomic Physics, Tata Institute of Fundamental Research, Mumbai 400005, India*

[2]*Department of Physics, Indian Institute of Technology, Roorkee 247667, India*

[3]*Pelletron Linac Facility, Tata Institute of Fundamental Research, Mumbai 400005, India*

[4]*India-based Neutrino Observatory, Tata Institute of Fundamental Research, Mumbai 400005, India*

[5]*Nuclear Physics Division, Bhabha Atomic Research Centre, Mumbai 400085, India*

[6]*Variable Energy Cyclotron Centre, 1/AF Bidhannagar, Kolkata 700064, India*

[7]*Homi Bhabha National Institute, Anushaktinagar, Mumbai 400094, India*

(Received 15 April 2017; published 13 July 2017)

Exclusive measurements of high-energy γ rays have been performed in ^{124}Ba and ^{136}Ba at the same excitation energy (∼49 MeV) to study the properties of the giant dipole resonance (GDR) over a wide N/Z range. The high-energy γ rays are measured in coincidence with the multiplicity of low-energy γ rays to disentangle the effect of temperature (T) and angular momentum (J). The GDR parameters are extracted employing a simulated Monte Carlo statistical model analysis. The observed γ-ray spectra of ^{124}Ba can be explained with prolate deformation, whereas a single-component Lorentzian function which corresponds to a spherical shape could explain the γ-ray spectra of ^{136}Ba. The observed GDR width in ^{136}Ba is narrower compared to that of ^{124}Ba. The statistical model best-fit GDR cross sections are found to be in reasonable agreement with the thermal shape fluctuation model (TSFM) calculations. Further, it is shown that the variation of GDR width with T is well reproduced by the TSFM calculations over the temperature range of 1.1–1.7 MeV.

DOI: 10.1103/PhysRevC.96.014309

I. INTRODUCTION

The isovector giant dipole resonance (GDR) is an excellent probe to study the collective behavior of the nucleus [1–6]. Using the GDR built on excited states (hot GDR) (produced via fusion-evaporation/inelastic scattering reactions/fission), the evolution of nuclear shape and damping mechanisms have been studied over a range of excitation energies (E^*) and angular momenta (J) across the nuclear chart. Recent studies in ^{130,132}Sn nuclei [7] together with an earlier measurement in ^{124}Sn nucleus [8] (spanning $N/Z = 1.48$–1.64) showed significant differences in the dipole ($E1$) strength distribution. The occurrence of the pygmy dipole resonance (PDR), a resonancelike concentration of $E1$ strength above the neutron threshold energy, has been confirmed in the exotic nuclei ^{130,132}Sn [7]. It would be interesting to see the effect of N/Z asymmetry on $E1$ strength distributions in other nuclei having a large variation of N/Z ratio. The barium isotopic chain ($A = 120$–144) having a wide N/Z ratio (1.14 to 1.57) and a significant variation of ground-state deformation ($\beta_{gs} = 0.09$–0.35 [9]), provides an opportunity to study the GDR over a large isospin asymmetry. Earlier, Vojtech *et al.* [10] reported the measurement of inclusive γ-ray spectra in the decay of ^{124}Ba and ^{136}Ba nuclei produced using ^{12}C + ^{112}Sn and ^{12}C + ^{124}Sn reactions, respectively, at beam energies of 7.5 and 10.5 MeV/nucleon. They have observed a single-component GDR indicative of spherical shape for both the nuclei with a large width of ∼8 MeV, even though these nuclei are known to be deformed in the ground state with $\beta_{gs} = 0.301$ and 0.1239 for ^{124}Ba and ^{136}Ba, respectively [9]. Further, significant enhancement was observed in the γ-ray yield beyond 20 MeV for the ^{136}Ba nucleus, speculated to originate due to a neutron skin in ^{136}Ba. It should be noted that in the $A \sim 130$ region, a few measurements are reported addressing the saturation of the GDR width at high excitation energies in ^{132}Ce [11] and in ^{136}Xe [12]. However, at these excitation energies the observed GDR widths have additional contributions from factors like the compound nuclear lifetime. Data at lower excitation energies are desirable for $A \sim 130$ nuclei, for comparison with thermal shape fluctuation model (TSFM) predictions, which is the most successful model describing the temperature dependence of the GDR width in excited nuclei [13–17].

With this motivation, ^{12}C + ^{112}Sn [at $E(^{12}\text{C}) = 64$ MeV] and ^{12}C + ^{124}Sn [at $E(^{12}\text{C}) = 52$ MeV] reactions are performed to study the GDR in ^{124}Ba and ^{136}Ba nuclei, respectively, at the same excitation energy ∼49 MeV. The choice of lower excitation energy ensured that contributions from preequilibrium emission and nucleon-nucleon bremsstrahlung are expected to be negligible and will not affect the GDR spectra, enabling a cleaner comparison with TSFM. The high-energy γ rays are detected in coincidence with low-energy γ rays for decoupling the temperature and angular momentum effects on the GDR parameters. The experimental GDR strength functions are compared with the GDR strength functions calculated using a thermal shape fluctuation model [13–17], where the angular momentum and temperature dependence of shell effects are included. The GDR widths from the present measurement are combined with those from the earlier measurements [10] to see the GDR width variation over a wide T range. This paper is organized as follows. Section II

*Present address: Department of Physics, National Institute of Technology Karnataka, Surathkal - 575025, India.

†nanal@tifr.res.in

describes the details of the experiment and simulations of the detector response using the GEANT4 tool kit, followed by the statistical model analysis for extracting the GDR parameters in Sec. III. The details of the TSFM calculation are presented in Sec. IV. In Sec. V, results of the GDR strength function and comparison with the TSFM calculations are discussed. Finally, the summary and conclusion are presented in Sec. VI.

II. EXPERIMENTAL DETAILS

Pulsed ^{12}C beams of energies 64 and 52 MeV from the Pelletron Linac Facility (PLF), Mumbai, India, were used for GDR studies in ^{124}Ba and ^{136}Ba nuclei at the same excitation energy ($\sim$49 MeV) employing self-supporting ^{112}Sn (2.3 mg/cm^2) and ^{124}Sn (1.9 mg/cm^2) targets, respectively. The detector system used for high-energy γ-ray measurement is similar to that described in Ref. [18]. High-energy γ rays were detected in an array of seven close-packed hexagonal BaF_2 detectors (each having face-to-face distance of 9 cm and length of 20 cm) placed at a distance of $\sim$57 cm from the target and at an angle of 125° with respect to the beam direction. The array was surrounded with an annular plastic scintillator for cosmic ray rejection. The entire detector setup (BaF_2 + plastic) was surrounded by a 10-cm-thick lead for attenuating ambient and beam-induced γ-ray background. In addition, a 5-mm-thick lead sheet was mounted on the front face of the BaF_2 array for reducing low-energy γ-ray and x-ray background. The beam dump was $\sim$2 m away from the target and was properly shielded with borated paraffin and lead for reducing the neutron and γ-ray background, respectively. The time of flight (TOF) of each BaF_2 detector with respect to the RF pulse was used to separate neutron and γ-ray induced events. The typical full width at half maximum (FWHM) of the γ-ray prompt peak in the TOF spectrum is $\sim$2 ns. Each detector anode signal was integrated over two different gates: 2 μs, referred to as $Q_{\rm long}$, and 200 ns, referred to as $Q_{\rm short}$, for energy measurement and pileup rejection using pulse shape discrimination, respectively. The array was calibrated using ^{137}Cs, ^{60}Co, and ^{241}Am-^{9}Be radioactive sources covering the energy range 0.6–4.4 MeV. The higher-energy calibration points (18.1 and 22.6 MeV) were obtained by bombarding a $\sim$1 mg/cm^2 thick ^{11}B target (prepared by electrodeposition on a 127-μm-thick tantalum backing) by a proton beam of energy 7.2 MeV [19]. During the experiment, the gain of the BaF_2 detectors were periodically monitored using radioactive sources and the variation was found to be within $\pm$2%.

The energy response of the array was generated using the GEANT4 [20]-based simulation employing the actual detector configuration in the present experiment. The simulated energy spectra of each detector were convoluted with a Gaussian resolution function for comparison with the measured γ-ray spectra from sources and the ^{11}B(p,γ) reaction, where the FWHM of the Gaussian function was optimized to fit the experimental spectra. The resolution (FWHM/E) was found to vary as $1/\sqrt{E}$ with a typical value of $\sim$6% at 22 MeV. For a given incident energy, the individual detector spectra folded with the resolution function were added to generate the total energy spectrum and the response matrix of the array was constructed for a range of γ-ray energies E_γ = 1 to 30 MeV.

In the present measurement, the angular momentum of the compound nucleus (CN) is extracted from the multiplicity of low-energy γ rays. An array of 14 element hexagonal bismuth germanate (BGO) detectors (each having 5.6 cm face-to-face distance and length of 7.6 cm), arranged in castle geometry above and below the target chamber (7 + 7), was used as the multiplicity filter. Fold, the number of BGO detectors fired above 120-keV threshold within a 50-ns coincidence window, is a measure of the multiplicity and is recorded for each event. The logic "OR" of the (time-matched) timing signals from top and bottom BGOs is used for TOF (BGO_TOF) measurement with respect to the RF pulse. This is also used for subtracting the chance coincident events in the multiplicity filter. The multiplicity to fold response of the array depends on the efficiency and the cross talk of the array. The efficiency of the array was measured using a calibrated ^{137}Cs source placed at the target position and found to be 64.2 $\pm$ 0.2%. The cross talk was obtained in a coincidence measurement using a ^{60}Co source placed at the target position and a $CeBr_3$ detector (cylindrical: 38 $\times$ 38 mm) placed outside of the target chamber. The measured cross-talk probability at this energy is $\sim$9%. The response of the multiplicity filter was also calculated by GEANT4-based Monte Carlo simulations. The simulated efficiency (63%) at 662 keV and the cross-talk probability (8%) at 1.2 MeV are in good agreement with measurements.

The master trigger was generated when the sum energy deposited in the BaF_2 array was above $\sim$5 MeV. Parameters recorded for each event were $Q_{\rm short}$, $Q_{\rm long}$, TOF of each BaF_2 (BaF_TOF) detector, BGO_TOF, and fold (F). Event-by-event data were acquired using a Computer Automated Measurement And Control (CAMAC) based acquisition-cum-analysis software LAMPS [21] for 0.23 and 0.63 pmC of incident beam particles in ^{12}C + ^{112}Sn and ^{12}C + ^{124}Sn reactions, respectively.

In the offline analysis, the $Q_{\rm long}$ for individual BaF_2 detector was filtered using the γ prompt in BaF_TOF and pileup rejection condition. The fold was also filtered using the prompt in BGO_TOF. Both the filtered $Q_{\rm long}$ and fold were corrected for the chance coincidences in BaF_TOF and BGO_TOF, respectively. The total energy spectrum was constructed by adding these corrected $Q_{\rm long}$ of individual detectors after calibration. The spectrum is further corrected for the Doppler effect owing to finite recoil velocity of the CN corresponding to a mean angle of 125° for the average CN recoil velocity ($v/c \sim 0.01$).

The γ-ray spectra from the ^{12}C + ^{112}Sn reaction at 64 MeV and from the ^{12}C + ^{124}Sn reaction at 52 MeV, for the fold window 5–6, are shown in Fig. 1. From the events satisfying the present analysis conditions, a two-dimensional matrix of fold vs total energy was generated. Suitable projections of the matrix yielded desired fold-gated γ-ray spectra and energy-gated fold distributions.

The larger fusion cross sections of the beam with light mass impurities present in the target (mainly C and O) can give significant contributions in the high-energy γ-ray spectrum. The amount of ^{12}C and ^{16}O present in the target was estimated from the yield of 4.44- and 6.13-MeV γ rays in the resonance radiative proton capture reactions at $E_{\rm p}$ = 7.78 MeV [22] and at $E_{\rm p}$ = 7.46 MeV [23], respectively. The above reactions with

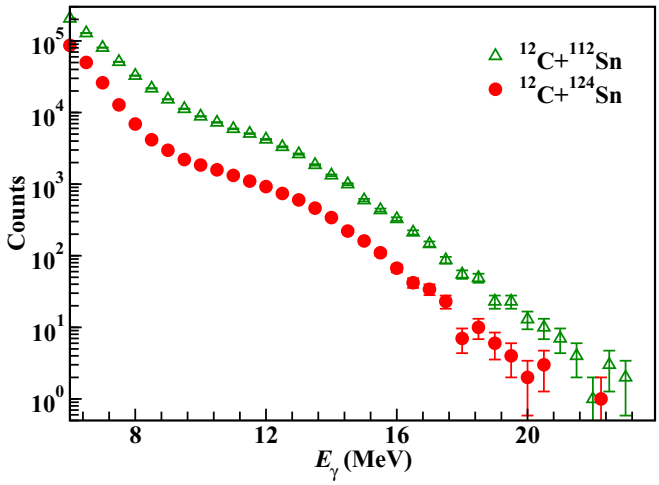

FIG. 1. The high-energy γ-ray spectra from the $^{12}C + ^{112}Sn$ reaction at 64 MeV (triangle) and from the $^{12}C + ^{124}Sn$ reaction at 52 MeV (solid circle), for the fold window 5–6.

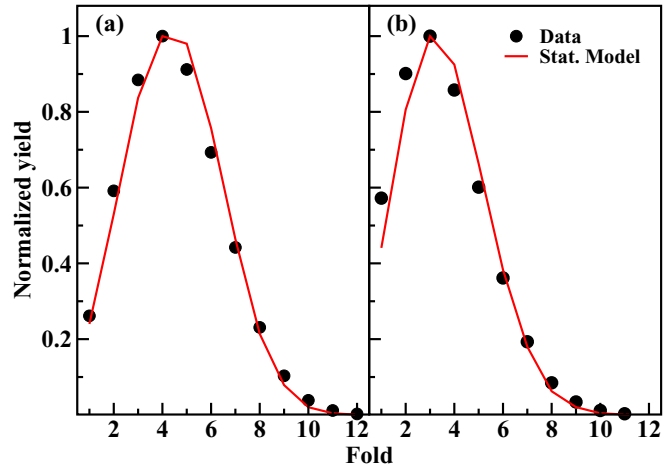

FIG. 2. The energy gated (10–20 MeV) experimental and simulated fold distribution for reactions: (a) $^{12}C + ^{112}Sn$, with $E(^{12}C) =$ 64 MeV, and (b) $^{12}C + ^{124}Sn$, with $E(^{12}C) = 52$ MeV.

^{12}C and WO_3 target were used as a reference for the 4.4- and 6.13-MeV γ-ray yield, respectively. From the ratios of the γ-ray yields from the reactions using the actual target, as well as ^{12}C and WO_3 targets, the carbon and oxygen impurities in the target were extracted and were found to be ~4% and ~14%, respectively. However, the contribution from these impurities at the fold-gated ($F > 3$) high-energy γ-ray spectrum was less than 1% and hence was ignored.

III. STATISTICAL MODEL ANALYSIS

The statistical model (SM) analysis has been carried out for extracting the GDR parameters from the experimental fold-gated high-energy γ-ray spectra. For generating the fold-gated γ-ray spectra, a simulated Monte Carlo CASCADE (SMCC) [24] code is used. The parameters used for calculating the particle transmission coefficients in the optical model potential are taken from Refs. [25–27]. Another important input for the SM calculation is the nuclear level density. For the present work, the level density formalism proposed by Ignatyuk *et al.* [28] is used with the asymptotic level density parameter $\tilde{a} = A/9.0$ MeV^{-1} for both ^{124,136}Ba nuclei. In these calculations, the CN is assumed to follow the standard angular momentum distribution,

$$\sigma(J_{CN}) = \sigma_0 \frac{2J_{CN}+1}{1+\exp[(J_{CN}-J_0)/\delta J]}, \qquad (1)$$

with $\delta J = 2$. The residue spin distribution (J_{res}) is calculated for each J_{CN} as a function of γ-ray energy by summing over all intermediate γ decays. The multiplicity (M) of low-energy γ rays for the decay from spin J_{res} to the ground state is calculated using the relative decay probability (P_r) of $\Delta J = 1$ and $\Delta J = 2$ transitions as a parameter. The multiplicity to fold response of the BGO array is constructed in a Monte Carlo approach incorporating the energy-dependent efficiency and cross-talk probability calculated using the GEANT4 simulation tool kit. By varying P_r, the experimental fold distributions in $^{12}C + ^{112}Sn$ and $^{12}C + ^{124}Sn$ reactions are reproduced and are shown in Fig. 2.

The best-fit GDR parameters for describing the different fold-gated γ-ray spectra are extracted following the same procedure as described in Ref. [18]. The photoabsorption cross section for an axially symmetric deformed (prolate or oblate) nucleus can be expressed by a two-component Lorentzian function as

$$\sigma_{abs}(E_\gamma) = \frac{4\pi e^2\hbar}{mc}\frac{NZ}{A}\sum_{j=1}^{j=2}\frac{S_j\Gamma_j E_\gamma^2}{\left(E_\gamma^2 - E_j^2\right)^2 + E_\gamma^2\Gamma_j^2}, \qquad (2)$$

where N and Z represent the neutron and proton numbers, $E_{1(2)}$, $\Gamma_{1(2)}$, and $S_{1(2)}$ are the centroids, widths, and strengths for the two components, respectively. For spherical nuclei, the oscillations along three mutually perpendicular axes are identical and a single-component Lorentzian in Eq. (2) can describe the observed GDR strength distribution. It is assumed that the GDR oscillation exhausts 100% ($S_1 + S_2 = 1$) of the Thomas-Reiche-Kuhn (TRK) sum rule [29]. In an earlier work we have shown that the extracted best-fit parameters remain unaffected within errors even with 25% variation of the TRK sum rule [18]. The experimental fold-gated γ-ray spectra are compared with the calculated spectra after folding the BaF_2 response function. Since the absolute γ-ray cross sections are not measured, both spectra are normalized at $E_\gamma = 8$ MeV. The χ^2 minimization and visual inspection in the energy range of 8–23 MeV are used to achieve the goodness of fit and to extract the best-fit GDR parameters.

From the projectile energy and the Q value of the reaction, the excitation energy of the compound nucleus is calculated. If E_{rot} and Δ_p are the rotational energy and pairing energy, respectively, then the net excitation energy available for internal excitation is $U = E_f^* - E_{rot} - \Delta_P$, where E_f^* is the excitation energy after the emission of the GDR γ ray. The temperature of the state on which the GDR is built, is calculated using the relation $U = aT^2$, where $a(U)$ is the Ignatyuk level density parameter [28]. The average temperature ($\langle T \rangle$) and angular momentum ($\langle J \rangle$) for different fold windows are calculated following the same procedure as in Ref. [18].

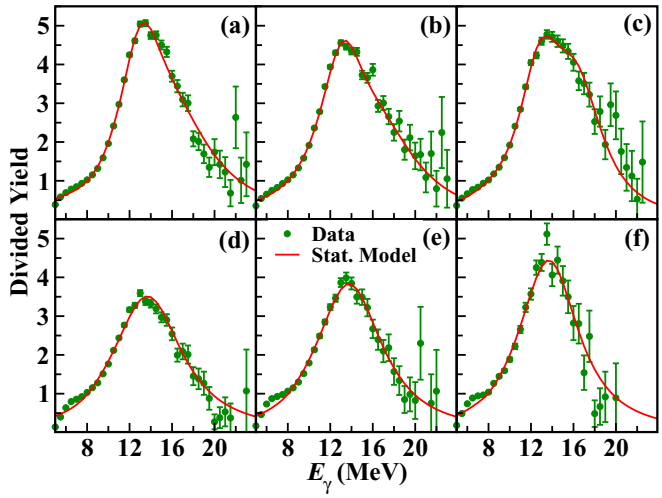

FIG. 3. Top panels show the divided plots for $^{12}C + ^{112}Sn$: (a) fold 3–4, (b) 5–6, and (c) 7–14. Bottom panels (d), (e), (f) show the same for $^{12}C + ^{124}Sn$. The line corresponds to the statistical model best-fit calculations.

For the present statistical model analysis, the γ-ray spectra are calculated considering prolate, oblate, and spherical shapes. In the earlier work [10] the high-energy γ-ray spectra from ^{124}Ba were described with a spherical shape in the statistical model, but the present data for ^{124}Ba could not be fitted with a single-component Lorentzian function. The γ-ray spectra of ^{124}Ba are found to be consistent with prolate deformation, whereas for ^{136}Ba a single-component Lorentzian function corresponding to a spherical shape could explain the data. The γ-ray spectrum calculated with an arbitrary constant dipole strength of 0.2 W.u., folded with the BaF_2 response, was used for generating divided plots for different folds. These plots for both the experimental and the calculated γ-ray spectra corresponding to different fold windows are shown in Fig. 3.

The best-fit parameters for ^{124}Ba are listed in Table I. In case of an axially symmetric deformed nucleus, the centroid of the GDR (E_D) is calculated as the weighted average of the centroid of two components and the effective GDR width (Γ_D) is taken as the full width at half maximum of the total GDR strength function. In Table II, the E_D, Γ_D, $\langle T\rangle$, $\langle J\rangle$, and deformation parameter (β) for ^{124}Ba are tabulated for different fold windows. For the ^{124}Ba nucleus, within the limited T and J range studied in the present experiment, the GDR centroid ($\sim$16 MeV), width ($\sim$8.0 MeV), and β remain constant.

TABLE I. Best-fit GDR parameters from SMCC analysis with prolate deformation for various fold windows for ^{124}Ba at $\sim$49 MeV excitation energy.

Fold	E_1 (MeV)	Γ_1 (MeV)	E_2 (MeV)	Γ_2 (MeV)	S_2
3–4	13.6(1)	3.7(2)	16.7(2)	9.0(4)	0.70(3)
5–6	13.7(1)	4.0(2)	17.5(3)	9.5(5)	0.67(3)
7–14	13.4(1)	3.7(2)	17.1(2)	5.9(3)	0.70(3)

TABLE II. Extracted GDR parameters and nuclear deformation β, as a function of J and T for prolate deformation for ^{124}Ba.

Fold	$\langle J\rangle$ ($\hbar$)	$\langle T\rangle$ (MeV)	E_D (MeV)	Γ_D (MeV)	β
3–4	14(7)	1.19(27)	15.8(2)	7.9(4)	0.24(2)
5–6	19(6)	1.16(25)	16.2(3)	8.8(5)	0.29(2)
7–14	22(6)	1.12(24)	16.0(2)	8.2(4)	0.29(2)

For ^{136}Ba, the extracted best-fit parameters for various fold windows are listed in Table III along with $\langle T\rangle$ and $\langle J\rangle$. In this case also, the centroids ($\sim$14.7 MeV) and the width are nearly constant in the present T and J range, and the width is significantly narrower (by $\sim$1 MeV) than that for ^{124}Ba. The observed centroid ($\sim$16 MeV) for ^{124}Ba is found to be in reasonable agreement with the ground-state systematics, whereas that for ^{136}Ba ($\sim$14.7 MeV) is marginally smaller than the systematics.

IV. TSFM CALCULATION

The free energy surfaces (FESs) for ^{124}Ba and ^{136}Ba nuclei have been calculated at the experimentally measured values of T and J and are shown in Figs. 4 and 5, respectively. The most probable shape (MPS) of the nucleus is represented by a solid dot. In the case of ^{124}Ba, at $T = 1.12$ MeV and $J = 22\hbar$ the nucleus prefers an oblate deformation with $\beta = 0.2$ and $\gamma = -180^\circ$. As T increases, our calculations suggest a shallow bottom with multiple minima in the FES. At $T = 1.16$ MeV and $J = 19\hbar$, the nucleus prefers an oblate shape with $\beta = 0.2$ and $\gamma = -170^\circ$ with an additional minimum in the FES at $\gamma = -80^\circ$. At $T = 1.19$ MeV and $J = 14\hbar$, the nucleus acquires a near triaxial shape with $\beta = 0.2$ and $\gamma = -160^\circ$, with a coexisting minimum in the FES. The deformation parameter β remains constant at all measured T values. At higher T values, the area spanned by the first and second minimum contour lines is large. However, the area covered by these contour lines lies in the lower β regions. This leads to a decrease in the average deformation values even if there is an increase in the thermal shape fluctuations. For the ^{136}Ba nucleus, the FESs (shown in Fig. 5) are more crisp and the shape of the nucleus remains spherical in the measured range of T and J.

The thermal fluctuations related to the shape degrees of freedom at a finite excitation energy are large in nuclei. The thermal shape fluctuations (TSFs) carry information about the shape rearrangements [14] at finite excitation energy. The general expression for the average value of GDR cross section

TABLE III. Best-fit GDR parameters from SMCC analysis with prolate deformation for various fold windows for ^{136}Ba at $\sim$ 49 MeV excitation energy.

Fold	$\langle J\rangle$ ($\hbar$)	$\langle T\rangle$ (MeV)	E_D (MeV)	Γ_D (MeV)
3–4	11(5)	1.24(28)	14.7(2)	7.4(3)
5–6	13(5)	1.23(28)	14.7(2)	7.0(3)
7–14	15(5)	1.22(29)	14.5(2)	6.2(3)

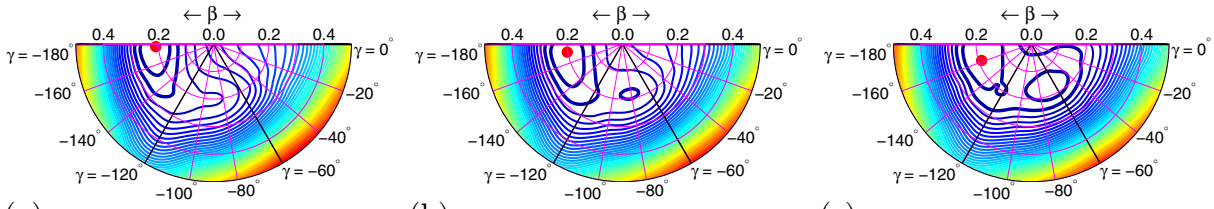

(a) $T = 1.12$ MeV, $J = 22\hbar$ (b) $T = 1.16$ MeV, $J = 19\hbar$ (c) $T = 1.19$ MeV, $J = 14\hbar$

FIG. 4. The free energy surfaces (FESs) of ^{124}Ba at different temperature (T) and angular momentum (I) combinations corresponding to the data measured at beam energy $E \sim 64$ MeV. In this convention, $\gamma = 0^\circ$ and -120° represent the noncollective and collective prolate shapes, respectively; $\gamma = -180^\circ$ and -60° represent the noncollective and collective oblate shapes, respectively. The contour line spacing is 0.2 MeV. The most probable shape is represented by a solid circle and the first two minima are represented by thick lines.

σ, incorporating such TSF has the form [15,30]

$$\langle\sigma(T,J)\rangle_{\beta,\gamma} = \frac{\int_\beta\int_\gamma \mathcal{D}[\alpha]\exp\left[-F_{\rm TOT}(T,J;\beta,\gamma)/T\right]\Im_{\rm TOT}^{-3/2}\sigma(J;\beta,\gamma)}{\int_\beta\int_\gamma \mathcal{D}[\alpha]\exp\left[-F_{\rm TOT}(T,J;\beta,\gamma)/T\right]\Im_{\rm TOT}^{-3/2}}, \quad (3)$$

with the volume element given by $\mathcal{D}[\alpha] = \beta^4|\sin 3\gamma|d\beta d\gamma$. $F_{\rm TOT}$ is the free energy calculated by microscopic-macroscopic method with proper T- and J-dependent shell corrections and $\Im_{\rm TOT}$ is the moment of inertia.

We employ a macroscopic approach for the GDR to relate the GDR observables and nuclear shapes [16,31,32]. The GDR Hamiltonian could be written as a sum of the anisotropic harmonic oscillator Hamiltonian and the separable dipole-dipole interaction,

$$H = H_{\rm osc} + \eta D^\dagger D. \quad (4)$$

The value of the dipole-dipole interaction strength η was varied to get the best fit to data ($E_\gamma = 8$ to 23 MeV) and is chosen as 2.9 for ^{124}Ba and 2.8 for ^{136}Ba, respectively.

V. RESULTS AND DISCUSSION

The comparison of fold-gated GDR spectra in ^{124}Ba and ^{136}Ba, presented in the earlier section, brings out significant differences between these two nuclei. The spherical shape of ^{136}Ba could be a manifestation of a nearly closed shell $N = 82$ and is also consistent with the FES calculations as can be seen in Fig. 5. For ^{124}Ba, the $\beta \sim 0.29(2)$ obtained from the SM analysis is similar to $\beta_{\rm gs} = 0.301$ [9]. This is not surprising since the yrast like deformation is expected to persist up to $T_{\rm lim} \sim 40\delta A^{-1/3}$ [33] (where $\delta \approx 0.95\beta$), which is $\sim$2 MeV for ^{124}Ba. However, the TSFM predicts the equilibrium deformation to be oblate.

For comparison of the data with TSFM, the procedure described in Ref. [18] is followed, where the experimental GDR cross section ($\sigma_{\rm stat}$) represented by the photoabsorption cross section used as input in the SM analysis [Eq. (2)], is compared with the calculated GDR cross section using TSFM ($\sigma_{\rm TSFM}$). For each fold window, the $\sigma_{\rm stat}$ is calculated using the best-fit parameters and is normalized to $\sigma_{\rm TSFM}$ in the $E_\gamma = 8$- to 23-MeV range, since the absolute GDR cross section is not measured. The comparison of $\sigma_{\rm stat}$ and $\sigma_{\rm TSFM}$ for ^{124}Ba and ^{136}Ba is shown in the top and bottom panels of Fig. 6, respectively, for different fold windows. The error bars in $\sigma_{\rm stat}$ represent the variation of $\sigma_{\rm stat}$ calculated from the errors of best-fit parameters.

It is evident that for ^{136}Ba the agreement with TSFM is good. For ^{124}Ba, some differences are seen in the shape of the strength function since the FES predicts the equilibrium shape as oblate (see Fig. 4). However, the observed effective GDR width is in reasonable agreement with that obtained from the TSFM calculation. The $\Gamma_{\rm D}$ in ^{136}Ba is significantly narrower ($\sim$15%) compared to that in ^{124}Ba, emphasizing the dominant role of fluctuations owing to the shallow minima in the FES (Fig. 4) in the latter case.

From earlier measurement by Vojtech *et al.* [10], it was found that $\Gamma_{\rm D}$ in ^{124}Ba and ^{136}Ba are similar at higher excitation energy. To compare the GDR widths from the inclusive measurements of earlier data [10], the average temperatures (T) after the GDR emission are calculated for the compound nuclei ^{124,136}Ba following the procedure described in Refs. [34,35]. The net energy available for internal excitation for these nuclei after the GDR γ-ray emission is calculated

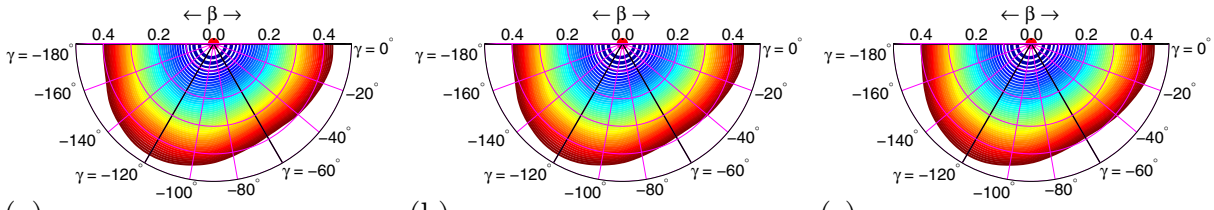

(a) $T = 1.22$ MeV, $J = 15\hbar$ (b) $T = 1.23$ MeV, $J = 13\hbar$ (c) $T = 1.24$ MeV, $J = 11\hbar$

FIG. 5. Same as Fig. 4, but for ^{136}Ba.

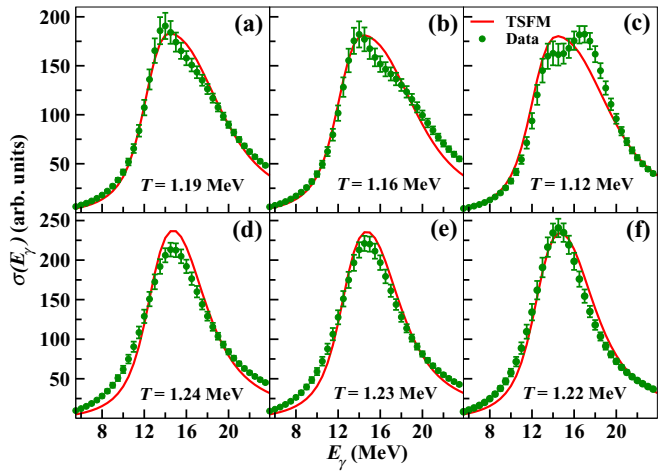

FIG. 6. Comparison of σ_{stat} and σ_{TSFM} for fold windows 3–4, 5–6, and 7–14 for the $^{12}\text{C} + ^{112}\text{Sn}$ reaction at $E(^{12}\text{C}) = 64$ MeV [in the top panels (a),(b),(c)] and for the $^{12}\text{C} + ^{124}\text{Sn}$ reaction at $E(^{12}\text{C}) = 52$ MeV [in the bottom panels (d),(e),(f)].

by subtracting the energy loss due to preequilibrium particle emission [36] and the rotational energy. The rotational energies are calculated using the moment of inertia of a symmetrically deformed nuclei with the respective ground-state deformation. It should be mentioned that we obtain a lower value of T for $E(^{12}\text{C}) = 127$ MeV, as compared to Fig. 3 in Ref. [11], owing to incorporation of the preequilibrium emission.

The Γ_{D} for ^{124}Ba (^{136}Ba) from the present (filled symbols) and earlier measurements ("*" symbols) are shown as a function of T in the top (bottom) panel of Fig. 7 together with Γ_{TSFM} (open symbols). The error bars in the Γ_{TSFM} correspond to the variation resulting from the experimental

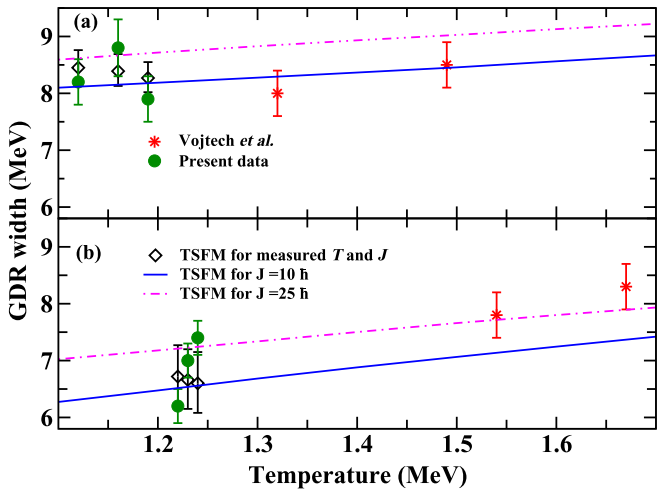

FIG. 7. The variation of Γ_{GDR} with temperature for (a)^{124}Ba and (b)^{136}Ba together with Γ_{TSFM} (open symbols). The error bars in the Γ_{TSFM} correspond to the variation resulting from the experimental spread in temperature. The "*" symbols represent the data taken from Vojtech *et al.* [10]. The prediction of Γ_{TSFM} for $J = 10\hbar$ (continuous line) and for $J = 25\hbar$ (dash-dotted line), corresponding to angular momentum range spanned by data, are also shown for comparison.

spread in T. Within the experimental errors, the observed Γ_{D} is in good agreement with the TSFM calculations. This figure also shows Γ_{TSFM} as a function of T for $J = 10\hbar$ and $J = 25\hbar$, corresponding angular momentum range spanned by the data. The calculated widths are in reasonable agreement with the data for both the nuclei over the temperature range of 1.1–1.7 MeV. It should be noted that at given T-J, the Γ_D (^{136}Ba) is smaller than the Γ_{D} (^{124}Ba), but the increase in Γ_{D} with T appears to be more rapid in ^{136}Ba than in the case of ^{124}Ba. This is perhaps indicative that the near shell closure effect plays a dominant role at low temperature in ^{136}Ba. The advent of radioactive ion beam facilities and modern detection systems will facilitate GDR studies in nuclei with wider N/Z ratios in near future.

VI. SUMMARY AND CONCLUSION

Exclusive measurements of high-energy γ rays have been performed for ^{124}Ba and ^{136}Ba at the same excitation energy (∼49 MeV) to study properties of the giant dipole resonance (GDR) over a wide N/Z range. The multiplicity of low-energy γ rays is measured in coincidence with high-energy γ rays to disentangle the effects of T and J. The GDR parameters are extracted employing a simulated Monte Carlo statistical model analysis. The observed γ-ray spectra of ^{124}Ba can be explained with prolate deformation with $\langle\beta\rangle = 0.29$, which is very similar to the ground-state deformation. The observed GDR centroid (∼16 MeV) and width (∼8 MeV) remain constant for the studied T (1.12–1.19 MeV) and J (14$\hbar$–22$\hbar$) ranges. In the case of ^{136}Ba, a single-component Lorentzian function that indicates a spherical shape explains the γ-ray spectra very well. In this case also, no significant variations (beyond experimental errors) are observed in the centroid energy ∼14.7 MeV and the width ∼7.0 MeV. The observed variation in E_{GDR} for ^{124}Ba and ^{136}Ba is consistent with the systematics, but the width in the latter is considerably narrower. For both ^{124}Ba and ^{136}Ba, the width of the GDR is nearly constant in the T–J range studied and is in reasonable agreement with the TSFM calculations. Further, it is shown that the variation of Γ_{D} with T is well reproduced by the TSFM calculations over the temperature range of 1.1–1.7 MeV, predicting a faster increase for ^{136}Ba. Further studies for very neutron-rich barium isotopes with upcoming radioactive ion beam facilities would be interesting to probe the variation of GDR properties over a wider range of N/Z asymmetry.

ACKNOWLEDGMENTS

We thank K.V. Divekar, M.E. Sawant, S.C. Nadkar and R. Kujur for their assistance during setup, D. Pujara, R.D. Turbhekar for target preparation, and the Pelletron Linac Facility staff for smooth operation of the accelerator. The authors are grateful to Dr. D.R. Chakrabarty for help with the analysis programs and valuable discussions. A.K.R.K acknowledges RIKEN Supercomputer HOKUSAI GreatWave System, where the numerical calculations were carried out. P.A. acknowledges financial support from the Science and Engineering Research Board (India), SR/FTP/PS-086/2011 and DST/INT/POL/P-09/2014.

[1] K. A. Snover, Annu. Rev. Nucl. Part. Sci. **36**, 545 (1986).
[2] J. J. Gaardhøje, Annu. Rev. Nucl. Part. Sci. **42**, 483 (1992).
[3] A. Schiller and M. Thoennessen, At. Data Nucl. Data Tables **93**, 549 (2007).
[4] D. R. Chakrabarty, N. D. Dang, and V. M. Datar, Eur. Phys. J. A **52**, 143 (2016).
[5] B. L. Berman and S. C. Fultz, Rev. Mod. Phys. **47**, 713 (1975).
[6] J. Speth and A. Van der Woude, Rep. Prog. Phys. **44**, 719 (1981).
[7] P. Adrich *et al.*, Phys. Rev. Lett. **95**, 132501 (2005).
[8] S. C. Fultz, B. L. Berman, J. T. Caldwell, R. L. Bramblett, and M. A. Kelly, Phys. Rev. **186**, 1255 (1969).
[9] www.nndc.bnl.gov
[10] R. J. Vojtech, R. Butsch, V. M. Datar, M. G. Herman, R. L. McGrath, P. Paul, and M. Thoennessen, Phys. Rev. C **40**, R2441 (1989).
[11] O. Wieland *et al.*, Phys. Rev. Lett. **97**, 012501 (2006).
[12] G. Enders *et al.*, Phys. Rev. Lett. **69**, 249 (1992).
[13] Y. Alhassid, B. Bush, and S. Levit, Phys. Rev. Lett. **61**, 1926 (1988).
[14] Y. Alhassid and B. Bush, Nucl. Phys. A **509**, 461 (1990).
[15] Y. Alhassid, Nucl. Phys. A **649**, 107c (1999).
[16] P. Arumugam, G. Shanmugam, and S. K. Patra, Phys. Rev. C **69**, 054313 (2004).
[17] M. Gallardo, M. Diebel, T. Døssing, and R. A. Broglia, Nucl. Phys. A **443**, 415 (1985).
[18] C. Ghosh, G. Mishra, A. K. R. Kumar, N. Dokania, V. Nanal, R. G. Pillay, S. Kumar, P. C. Rout, S. Joshi, and P. Arumugam, Phys. Rev. C **94**, 014318 (2016).
[19] F. E. Cecil, D. Ferg, H. Liu, J. C. Scorby, J. A. McNeil, and P. D. Kunz, Nucl. Phys. A **539**, 75 (1992).
[20] S. Agostinelli *et al.*, Nucl. Instrum. Methods Phys. Res., Sect. A **506**, 250 (2003).
[21] www.tifr.res.in/∼pell/lamps.html
[22] A. C. L. Barnard, J. B. Swint, and T. B. Clegg, Nucl. Phys. **86**, 130 (1966).
[23] R. L. Dangle, L. D. Oppliger, and G. Hardie, Phys. Rev. **133**, B647 (1964).
[24] D. R. Chakrabarty, Nucl. Instrum. Methods Phys. Res., Sect. A **560**, 546 (2006).
[25] D. Wilmore and P. E. Hodgson, Nucl. Phys. **55**, 673 (1964).
[26] F. G. Perey, Phys. Rev. **131**, 745 (1963).
[27] L. McFadden and G. R. Satchler, Nucl. Phys. **84**, 177 (1966).
[28] A. V. Ignatyuk, G. N. Smirenkin, and A. S. Tishin, Sov. J. Nucl. Phys. **21**, 255 (1975).
[29] W. Thomas, Naturwissenschaftern **13**, 627 (1925); W. Kuhn, Z. Phys. **33**, 408 (1925); F. Reiche and W. Thomas, *ibid.* **34**, 510 (1925).
[30] Y. Alhassid and B. Bush, Nucl. Phys. A **531**, 39 (1991).
[31] G. Shanmugam and M. Thiagasundaram, Phys. Rev. C **37**, 853 (1988).
[32] A. K. R. Kumar, P. Arumugam, and N. D. Dang, Phys. Rev. C **91**, 044305 (2015).
[33] S. Bjornholm, A. Bohr, and B. R. Mottelson, Proc. 3rd IAEA Symp. on Phys. Chem. of Fission **1**, 367 (1973).
[34] A. Bracco, F. Camera, O. Wieland, and W. E. Ormand, Mod. Phys. Lett. A **22**, 2479 (2007).
[35] S. Bhattacharya, D. Pandit, S. Mukhopadhyay, S. Pal, and S. R. Banerjee, Phys. Rev. C **78**, 064601 (2008).
[36] M. P. Kelly, K. A. Snover, J. P. S. van Schagen, M. Kicińska-Habior, and Z. Trznadel, Phys. Rev. Lett. **82**, 3404 (1999).